The American Journal of Pathology, Vol. 195, No. 10, October 2025

ELSEVIER

The American Journal of
PATHOLOGY

ajp.amjpathol.org

GASTROINTESTINAL, HEPATOBILIARY, AND PANCREATIC PATHOLOGY

Peroxisome Proliferator–Activated Receptor Agonist IVA337 Alleviates Inflammation and Fibrosis in MASH by Restoring Lipid Homeostasis

Na Li,[*] Shuai Wu,[†] Xiaodan Li,[*] Meng Yan,[‡§] Yifu Ding,[‡§] Lingjuan Zhang,[†] David A. Brenner,[¶] Xiao Liu,[‖] and Tatiana Kisseleva[‖]

From the Shanghai University of Medicine & Health Sciences Affiliated Zhoupu Hospital,[*] School of Medical Technology, Shanghai University of Medicine & Health Sciences, Shanghai, China; State Key Laboratory of Cell Stress Biology,[†] School of Life Sciences, Xiamen University, Xiamen, China; State Key Laboratory of Cell Biology,[‡] Shanghai Key Laboratory of Molecular Andrology, Shanghai, China; Shanghai Institute of Biochemistry and Cell Biology,[§] Center for Excellence in Molecular Cell Science, Chinese Academy of Sciences, Shanghai, China; Sanford Burnham Prebys Medical Discovery Institute,[¶] La Jolla, California; and the Department of Surgery,[‖] University of California San Diego, La Jolla, California

Accepted for publication June 12, 2025.

Address correspondence to Na Li, Ph.D., Shanghai University of Medicine & Health Sciences Affiliated Zhoupu Hospital, No. 1500 Zhouyuan Rd., Shanghai, 201318, China; or Tatiana Kisseleva, M.D., Ph.D., Department of Surgery, University of California, San Diego, 9500 Gilman Dr., #0063, La Jolla, CA 92093. E-mail: lin_18@sumhs.edu.cn or tkisseleva@health.ucsd.edu.

Metabolic dysfunction–associated steatohepatitis (MASH), an advanced stage of metabolic dysfunction–associated steatotic liver disease, is characterized by significant hepatic fibrosis and inflammation. The pan-peroxisome proliferator–activated receptor (pan-PPAR) agonist IVA337 (lanifibranor) has shown potential as an anti-MASH therapeutic, although its mechanisms of action remain incompletely understood. This study explores the effects and mechanisms of IVA337 using two distinct MASH models: two-dimensional (2D) primary human hepatic stellate cells (HSCs) stimulated with transforming growth factor β1 (TGF-β1), and three-dimensional (3D) liver spheroids comprising primary hepatocytes, HSCs, and non-parenchymal cells. In TGF-β1–stimulated HSCs, IVA337 effectively suppressed the expression of fibrosis-related genes, including *PAI1*, *COL1A1*, and *ACAT2*, as well as the inflammatory gene *IL6*. 3D mouse and human liver spheroid models of MASH, characterized by elevated fibrotic gene expression, were established. IVA337 treatment not only attenuated fibrotic gene expression but also restored lipid content in the MASH spheroids, as evidenced by BODIPY staining. Immunostaining further confirmed a reduction in α-smooth muscle actin and collagen 1 levels after IVA337 treatment. Bulk RNA sequencing and Gene Ontology analysis revealed several lipid metabolism–related genes as key effectors downstream of IVA337. In addition, IVA337 modulated multiple signaling pathways, including IL-17, tumor necrosis factor, NF-κB, phosphatidylinositol 3 kinase/protein kinase B, and mitogen-activated protein kinase. Collectively, these findings show that IVA337 effectively mitigates fibrosis development in both 2D and 3D MASH models by restoring lipid homeostasis and regulating crucial fibrotic and inflammatory pathways. *(Am J Pathol 2025, 195: 1822–1838; https://doi.org/10.1016/j.ajpath.2025.06.012)*

Metabolic dysfunction–associated steatotic liver disease (MASLD), the most prevalent chronic liver disease, affects approximately 1 billion people worldwide. Characterized by a spectrum of liver abnormalities, MASLD can progress from simple steatosis (nonalcoholic fatty liver) to the more severe condition known as metabolic dysfunction–associated steatohepatitis (MASH) if risk factors such as obesity, dyslipidemia, oxidative stress, and diabetes are not mitigated.[1–3] MASH is defined by inflammation and hepatocyte death, potentially advancing to fibrosis, cirrhosis, and hepatocellular carcinoma.[4] Fibrosis is particularly critical, as it is a pivotal determinant of adverse clinical outcomes and mortality. Notably,

Sponsored by the National Natural Science Foundation of China (grant nos. 32293231 and 31900541) and Shanghai Pujiang Program (grant no. 21PJD027), and by the Shanghai Municipal Science and Technology Major Project.

https://doi.org/10.1016/j.ajpath.2025.06.012

fibrosis is the only histologic feature used to facilitate a clinical diagnosis of MASH.[5]

At the cellular level, the progression to fibrosis in MASH is driven by hepatic stellate cells (HSCs), which reside in the peri-sinusoidal spaces of the liver. Quiescent, vitamin A–rich HSCs are activated into a fibrogenic and pro-inflammatory state in response to complex signaling events emanating from lipid-laden hepatocytes and immune-derived inflammatory signals.[5–7] This scenario underscores the need to understand the molecular mechanisms driving fibrosis in MASH pathogenesis. Although the US Food and Drug Administration recently approved Rezdiffra (Resmetirom; Madrigal Pharmaceuticals, West Conshohocken, PA) for treating adults with MASH based on results from the Phase III MAESTRO-NASH [A Phase 3 Study to Evaluate the Efficacy and Safety of MGL-3196 (Resmetirom) in Patients With NASH and Fibrosis] trial, its use is limited in patients with decompensated cirrhosis or those requiring statins for cholesterol reduction.[8] Furthermore, the limited understanding of disease mechanisms highlights an urgent need for new MASH treatments compatible with lipid-lowering therapies.

Peroxisome proliferator–activated receptors (PPARs) play a pivotal role in regulating lipid metabolism, inflammation, oxidative stress, and energy homeostasis within the liver, aligning closely with metabolic dysfunctions such as MASLD. Comprising three isoforms, PPARα, PPARβ/δ, and PPARγ, which are encoded by the genes *PPARA, PPARD,* and *PPARG*, respectively, these nuclear transcription receptors exhibit distinct expression patterns and functional roles across different tissues.[9] PPARα mainly regulates fatty acid transport, beta-oxidation, and ketogenesis in the liver, whereas PPAR-β/δ is mainly expressed in the hepatocytes, macrophages, and skeletal muscle, and can inhibit insulin resistance in adipocytes.[10–16] PPARα suppresses pro-inflammatory cytokines and fibrogenic gene expression, thereby inhibiting HSC activation.[17] PPARβ/δ also contributes to the inhibition of HSC activation by attenuating inflammatory signaling and promoting HSC quiescence.[17] Although PPARγ1 is the only PPARγ isoform expressed in the liver and is primarily involved in lipogenesis and adipogenesis, PPARγ plays a crucial role in suppressing HSC activation and reducing collagen deposition during liver fibrogenesis, although its activity is often down-regulated during this process.[18] PPARs also interact with other transcription factors, such as liver X receptors and sterol regulatory-element binding proteins, to regulate lipogenesis, fatty acid oxidation, and triglyceride metabolism in the liver under physiological conditions.[19–23]

Given that all PPAR isotypes control the activation of HSCs and modulate glucolipid metabolism in MASLD, PPAR activation has been shown to prevent MASH progression via stimulating beta-oxidation and decreasing inflammation.[24] Various PPAR agonists have been evaluated in both animal models and clinical trials. For instance, fibrates (PPARα agonists) have shown potential for MASLD treatment, with extensive clinical trials pending.[25,26] PPARβ/δ agonists, such as GW501516 and GW0742, have been effective in ameliorating insulin resistance and reducing serum lipid levels in preclinical and human studies, albeit with limited long-term efficacy in clinical settings.[27] Pioglitazone, a PPARγ agonist, functions as both an anti-inflammatory and antifibrotic agent,[28] but other PPARγ agonists (troglitazone and rosiglitazone) have been associated with mild hepatotoxicity.[29,30]

To address these limitations, dual or pan-PPAR agonists have been proposed. Dual PPARα/γ agonists, for example, have shown efficacy in reducing liver inflammation and insulin resistance by modulating endoplasmic reticulum stress.[31,32] Elafibranor, a dual PPARα/δ agonist, has shown some benefits in resolving MASH in Phase II clinical trials.[33] In addition, the pan-PPAR agonist IVA337, which activates all PPAR subtypes,[34] has shown promise in both mouse models and human patients. In preclinical MASLD models, such as a methionine/choline–deficient diet and foz/foz mice in a high-fat diet, IVA337 significantly reduced inflammation and fibrosis.[35] Mechanistically, the beneficial metabolic effects of a pan-PPAR agonist counteracting inflammation and fibrosis was through directly modulating macrophage activation in MASLD.[36] Clinical Phase IIb trials involving patients with active MASH also reported beneficial effects of IVA337, suggesting potential success in forthcoming Phase III trials.[37]

Although PPAR agonists exhibit considerable therapeutic potential for MASLD and MASH, their underlying mechanisms remain poorly understood, partly because animal models fail to fully recapitulate human pathophysiology. The current study evaluated the effects of IVA337 on HSCs derived from patients with MASH and explored the molecular mechanisms involved. In addition, mouse and human three-dimensional (3D) MASH spheroids using primary cells have been developed to assess the roles of IVA337 and to identify key regulatory pathways. This comprehensive approach aims to bridge the gap between preclinical findings and clinical application, enhancing our understanding and treatment of this increasingly prevalent liver disease.

Materials and Methods

Primary Human HSC Culture and Treatment

Primary human HSCs (labeled as sc00 and sc55) were cultured in Dulbecco's modified Eagle's medium (C11965500BT; Thermo Fisher Scientific, Waltham, MA) supplemented with 10% fetal bovine serum (UT83998; Tocyto, Guangzhou, China) and 1% Antibiotic-Antimycotic (number 15240-062; Thermo Fisher Scientific). Human HSCs were stimulated with transforming growth factor-β1 (TGF-β1; 10 ng/mL) and IVA337 (20 mmol/L) for 24 hours, and analyzed by quantitative real-time PCR (qPCR).

3D Mouse and Human Spheroid Culture

3D human or mouse liver spheroids were generated as described in the published protocol with cryopreserved primary human hepatocytes or fresh isolated mouse primary hepatocytes, HSCs, and non-parenchymal cells (NPCs) at a ratio of 6:3:2 (hepatocytes:NPCs:HSCs) and 5000 viable cells per well into ultra-low attachment plates.[38] Human primary cells were generated from the human livers in previous studies, and mouse primary hepatocytes, HSCs, and NPCs were freshly isolated from chow diet–fed C57Bl6/J male mice (10 weeks of age; approximately 25 g) as described previously.[39,40]

The HSCs and NPCs used for generating human spheroids in this study were derived from a different MASH donor (labeled as 1116N) and were distinct from the HSCs used in the two-dimensional culture experiments. Furthermore, all human livers for generating primary cells in previous study were from deidentified livers, which were declined for transplantation and were obtained via the Lifesharing organ procurement organization. Patient consent was obtained by Lifesharing. This project (171883XX) has been reviewed by the Director of the University of California San Diego Human Research Protections Program, the Institutional Review Board Chair, or the Institutional Review Board Chair's designee. It was certified as not qualifying as human subjects research according to the Code of Federal Regulations, Title 45, Part 46, and the University of California San Diego Standard Operating Policies and Procedures, and it therefore does not require institutional review board review.

Livers were graded for steatosis, inflammation, and fibrosis by a pathologist using a double-blinded method[41] and identified as normal and MASH. Primary cells were then thawed and seeded in 200 μL Dulbecco's modified Eagle's medium supplemented with 1× Pen Strep, 1× ITS-G (Thermo Fisher Scientific), 40 ng/mL dexamethasone, and 10% fetal bovine serum. Spontaneous self-aggregation of the cells could initiate spheroid formation. From day 4 or 5 after seeding, when the spheroids were sufficiently compact, 50% of the medium was exchanged daily for serum-free medium. Spheroids were cultured in serum-free medium for 7 days and then treated with the MASH induction cocktail for another 7 days, followed by an additional 7-day treatment with either IVA337 or SB431542. Cultures were maintained until day 21, with medium changes every 48 to 72 hours. The spheroids were then harvested for further sequencing, qPCR, Western blot analysis, or immunofluorescence staining; the primers and antibodies used are listed in Tables 1 and 2, respectively.

RNA Extraction, Library Preparation, and Sequencing

Total RNA was extracted from human HSCs and pooled human spheroids (30 to 60 per group) using the RNeasy Micro Kit (Qiagen, Hilden, Germany). RNA integrity was assessed by using a Bioanalyzer (Agilent Technologies, Santa Clara, CA), and only samples with an RNA integrity number >7 were used for sequencing. Library preparation was performed with the Optimal Dual-mode mRNA Library Prep Kit [BGI (Shenzhen, China) and GENEWIZ (Suzhou, China)].

Briefly, RNA was denatured at an optimized temperature to disrupt secondary structures, and mRNA was selectively enriched using oligo(dT)–coated magnetic beads. After thermal incubation, RNA was fragmented by using a fragmentation buffer. First-strand cDNA synthesis was conducted by using random hexamer primers, followed by second-strand synthesis to generate double-stranded cDNA. The resulting cDNA was end-repaired, and a single "A" nucleotide was added to the 3′ ends via A-tailing. Adaptors were then ligated to the cDNA fragments, and the library was amplified by PCR and subjected to quality control.

Subsequently, the double-stranded libraries were denatured to produce single-stranded products. Circularization was performed to generate single-stranded circular DNA libraries, with uncyclized linear DNA digested enzymatically. Final circularized libraries were amplified by using phi29 DNA polymerase via rolling circle amplification to produce DNA nanoballs, each containing >300 copies of the original library molecule. DNA nanoballs were loaded onto patterned nanoarrays and sequenced by using paired-end 150 bp reads on the BGI T7 platform.

Low-quality reads, adapter sequences, and reads with excessive ambiguous bases (N) were filtered out to generate clean reads. These were aligned to the human reference genome (hg38) using HISAT2 version 2.2.1 (*https://daehwankimlab.github.io/hisat2*) and to reference genes using Bowtie2 version 2.4.5 (*https://bowtie-bio.sourceforge.net/bowtie2*). Gene expression quantification and differential expression analysis were performed by using RSEM version 1.3.1 (*https://github.com/deweylab/RSEM*). Hierarchical clustering and heatmap generation were conducted by using DESeq2 version 1.34.0 (*https://bioconductor.org/packages/release/bioc/html/DESeq2.html*). Functional enrichment analyses, including Gene Ontology, Gene Set Enrichment Analysis, and Kyoto Encyclopedia of Genes and Genomes (KEGG) pathway analysis, were conducted by using the clusterProfiler package in R version 3.10.1 (R Foundation for Statistical Computing, Vienna, Austria). All sequencing data have been uploaded to the Gene Expression Omnibus database (*https://www.ncbi.nlm.nih.gov/geo/query/acc.cgi?acc=*; accession number GSE292999).

Quantitative Real-Time PCR

qPCR was performed by using qTOWER3G (Analytik Jena AG, Jena, Germany). All the primers used in this study are listed in Table 1. Total RNA was isolated from mouse and human spheroids or human HSCs using Trizol and TRnaZol RNA Kit (NCM Biotech, Suzhou, China). Expression levels

Table 1 Quantitative Real-Time PCR Primers List

Number	Gene	Forward primer	Reverse primer
1	Human *ACTA2*	5′-CACCATCGGAAATGAACGTTT-3′	5′-GACTCCATCCCGATGAAGGA-3′
2	Human *COL1A1*	5′-AAGAGGAAGGCCAAGTCGAG-3′	5′-CACACGTCTCGGTCATGGTA-3′
3	Human *PAI1*	5′-ACCGCAACGTGGTTTTCTCA-3′	5′-TTGAATCCCATAGCTGCTTGAAT-3′
4	Human *CTGF*	5′-ACCCGGGTTACCAATGACAA-3′	5′-GTACGGATGCACTTTTTGCCC-3′
5	Human *IL6*	5′-AATTCGGTACATCCTCGACGG-3′	5′-TTGGAAGGTTCAGGTTGTTTTCT-3′
6	Human *ACLY*	5′-ATCGGTTCAAGTATGCTCGGG-3′	5′-GACCAAGTTTTCCACGACGTT-3′
7	Human *HMGCS1*	5′-CATTAGACCGCTGCTATTCTGTC-3′	5′-TTCAGCAACATCCGAGCTAGA-3′
8	Human *ACC1*	5′-ATGTCTGGCTTGCACCTAGTA-3′	5′-CCCCAAAGCGAGTAACAAATTCT-3′
9	Human *LDLR*	5′-GAATCTACTGGTCTGACCTGTCC-3′	5′-GGTCCAGTAGATGTTGCTGTGG-3′
10	Human *ABCA1*	5′-CAGGCTACTACCTGACCTTGGT-3′	5′-CTGCTCTGAGAAACACTGTCCTC-3′
11	Human *PLIN2*	5′-GATGGCAGAGAACGGTGTGAAG-3′	5′-CAGGCATAGGTATTGGCAACTGC-3′
12	Human *ANGPTL4*	5′-GTCCACCGACCTCCCGTTA-3′	5′-CCTCATGGTCTAGGTGCTTGT-3′
13	Human *ACAA2*	5′-AAGTCTCACCTGAAACAGTTGAC-3′	5′-CACGCAAACCAACATGCCT-3′
14	Human *FADS1*	5′-CCAACTGCTTCCGCAAAGAC-3′	5′-GCTGGTGGTTGTACGGCATA-3′
15	Human *CPT1A*	5′-ATCAATCGGACTCTGGAAACGG-3′	5′-TCAGGGAGTAGCGCATGGT-3′
16	Human *ACOT7*	5′-GGCCGGAAGCGGTATGAAG-3′	5′-GACTGGCTGTAGCTGACAGTG-3′
17	Human *NR4A1*	5′-ATACACCCGTGACCTCAACC-3′	5′-AGTCCTTGTTAGCCAGGCAG-3′
18	Human *MAP3K7CL*	5′-TGAGGTCAAAAAGGAAATCACCC-3′	5′-AACGTCCGATTCTCCTCCGT-3′
19	Human *PDGFA*	5′-ATACCTCGCCCATGTTCTGG-3′	5′-GCACATGCTTAGTGGCATGG-3′
20	Human *RASSF7*	5′-CAGGAAGTGGTCATCGCACT-3′	5′-ACACTCTTGTGGCAGCAACT-3′
21	Human *PLIN5*	5′-CCTTTCTCCAGCAACCTTCGGA-3′	5′-CAACATCCACAGCATGGCTCAC-3′
22	Human *CXCL8*	5′-GAGAGTGATTGAGAGTGGACCAC-3′	5′-CACAACCCTCTGCACCCAGTTT-3′
23	Human *CCL7*	5′-ACAGAAGGACCACCAGTAGCCA-3′	5′-GGTGCTTCATAAAGTCCTGGACC-3′
24	Human *MMP1*	5′-CTCTGGAGTAATGTCACACCTCT-3′	5′-TGTTGGTCCACCTTTCATCTTC-3′
25	Mouse *Acat2*	5′-GTTCAGTGGTGCCTCTGTCA-3′	5′-ACTGGGACGACATGGAAAAG-3′
26	Mouse *Il6*	5′-TGTGAAATGCCACCTTTTGA-3′	5′-GGTCAAAGGTTTGGAAGCAG-3′
27	Mouse *Fads1*	5′-AGCACATGCCATACAACCATC-3′	5′-TTTCCGCTGAACCACAAAATAGA-3′
28	Mouse *Scd1*	5′-CCAAGCTGGAGTACGTCTGG-3′	5′-CAGAGCGCTGGTCATGTAGT-3′
29	Mouse *Acot4*	5′-AGCAGTGCGGTACATGCTTC-3′	5′-AGAGCCATTGATGGAAACTGTG-3′
30	Mouse *Acaa2*	5′-ATGTGCGCTTCGGAACCAAA-3′	5′-CAAGGCGTATCTGTCACAGTC-3′
31	Mouse *Map3k7cl*	5′-TCGCATCGCGTTTAGCCTC-3′	5′-TGACTTCATGGTACTCTTCTGCT-3′
32	Mouse *Pcsk9*	5′-GAGACCCAGAGGCTACAGATT-3′	5′-AATGTACTCCACATGGGGCAA-3′

of selected genes were calculated versus the housekeeping gene HPRT using the $2^{-\Delta\Delta C_T}$ method.

Spheroid Immunofluorescence

Spheroids were transferred into 1.5 mL tubes, washed twice with phosphate-buffered saline (PBS), and fixed with 4% PFA for 1 hour at 37°C, followed by washing twice with PBS, for 5 minutes each. After fixation and PFA-quenching, samples were incubated in penetration buffer for 30 minutes, containing 0.2% Triton X-100, 0.3 mol/L glycine, and 20% dimethyl sulfoxide in PBS to improve penetration of antibodies and nuclear dyes. Spheroids were then washed twice with PBS and incubated in blocking buffer (0.2% Triton X-100, 6% donkey serum, and 10% dimethyl sulfoxide in PBS) for 2 hours at 37°C with gentle shaking. After blocking, samples were incubated with primary antibody (Table 2) in antibody buffer (0.2% Tween 20, 10 mg/mL heparin, 3% donkey serum, 5% dimethyl sulfoxide in PBS) overnight at 4°C with gentle shaking. Samples were then washed five times for 5 minutes each in washing buffer (0.2% Tween 20, 10 μg/mL heparin) and stained with secondary antibody and nuclear dyes overnight at 37°C with gentle shaking. Samples were washed subsequently five times for 5 minutes in washing buffer with gentle shaking and then cleared with an aqueous solution of 88% glycerol (refractive index of 1.459) at room temperature with gentle shaking. After mounting, spheroids were always kept in the microscope room for several hours to allow for temperature adjustment before microscopic examination.

Table 2 Antibodies List

No.	Antibody	Company	Catalog no.
1	HNF4A	Invitrogen (Carlsbad, CA)	MA1-199
2	Collagen 1	SouthernBiotech (Birmingham, AL)	1301-01
		Selleck Chemicals (Houston, TX)	F1228
3	α-SMA	Proteintech (Rosemont, IL)	14395-1-AP
4	PAI1	Proteintech	13801-1-AP
5	PLIN2	Proteintech	80362-2-RR
6	β-tubulin	Servicebio (Wuhan, China)	GB122667-100

α-SMA, α-smooth muscle actin; HNF4A, hepatocyte nuclear factor 4α.

For lipid staining, spheroids were transferred into 1.5 mL tubes, washed twice with PBS, and fixed with 4% paraformaldehyde for 1 hour at 37°C, followed by washing twice with PBS, for 5 minutes each. After fixation and PFA-quenching, samples were incubated with 2 um BODIPY 493/503 (GLPBIO, Montclair, CA) for lipids and 2.5 ug/mL DAPI for 1 hour at 37°C. The final lipid droplet volume was calculated by using Imaris 9.2.0 (Oxford Instruments, Abingdon, UK).

Immunocytochemistry

HSCs were fixed with 4% PFA for 10 minutes and then permeabilized with 0.1% saponin. Cells were blocked in 5% bovine serum albumin for 1 hour and subsequently incubated overnight at 4°C with primary antibodies as listed in Table 2. After washing, samples were incubated in the dark with appropriate Alexa Fluor 488–conjugated secondary antibodies for 4 hours at 4°C. Nuclei were counterstained with DAPI. Finally, cells were mounted by using ProLong Gold Antifade Mountant (Thermo Fisher Scientific) with DAPI. All images were acquired by using a Zeiss LSM880 confocal microscope (ZEISS Microscopy, Jena, Germany), and immunofluorescent intensity was quantified with ImageJ version 1.53t (NIH, Bethesda, MD; *https://imagej.net/ij*).

Statistical Analysis

All data represent the means ± SEM. Comparisons of two groups were analyzed by using an unpaired, two-tailed *t*-test. Comparisons of three or more groups were analyzed by using analysis of variance, and analysis of variance with a Dunnett test was used for comparing multiple groups of mice versus controls. $*P < 0.05$, $**P < 0.01$, $***P < 0.001$, and $****P < 0.0001$ was considered statistically significant and are indicated as such in the figure legends. All analyses were performed by using GraphPad Prism version 10.3.1 (GraphPad Software, La Jolla, CA).

Results

Pan-PPAR Agonist IVA337 Suppresses the Sustained Activation Phenotype of HSCs from Patients with MASH

HSCs are pivotal in the progression of MASH and become activated by diverse stimuli. In patients with MASH, persistent HSC activation results in excessive extracellular matrix deposition, culminating in fibrosis.[42] The therapeutic potential of the pan-PPAR agonist IVA337, previously reported in MASH murine models and undergoing clinical trials, prompted an investigation into its mechanistic role in modulating HSC activity in human MASH contexts.

Primary HSCs were isolated from liver biopsy specimens of patients with MASH. To delineate the effects of IVA337, SB431542, a selective TGF-β signaling inhibitor with established antifibrotic properties, was used as a control.[43] Cultured HSCs from MASH donors were treated with IVA337 or SB431542, following by RNA extraction for qPCR analysis to measure the expression of key fibrotic, inflammatory, and lipid regulatory markers.

Results revealed that IVA337 administration significantly reduced the expression of fibrotic markers such as *ACTA2* and *COL1A1* (approximately twofold reduction), as well as *PAI1* and *CTGF* (approximately threefold reduction), across donor samples. SB431542 displayed a similar inhibitory effect on these markers (Figure 1, A and B), and similar results were confirmed by Western blot analysis (Figure 1C). IVA337 uniquely down-regulated *IL6* by approximately twofold, an effect not observed with SB431542 (Figure 1, A and B). Given that aberrant lipid accumulation is a hallmark of MASH, the expression of key lipid metabolism–related regulatory genes after IVA337 and SB431542 treatment was also evaluated. Fatty acid synthesis regulators, *ACC1, ACLY*, and *FASN*, were up-regulated by both IVA337 and SB431542. Similarly, *LDLR,* which facilitates cholesterol uptake, was increased by both treatments. In contrast, *HMGCS1* (involved in cholesterol biosynthesis) and *ABCA1* (which mediates cholesterol efflux) were significantly up-regulated only in IVA337-treated cells but not in those treated with SB431542 (Figure 1, A and B).

Collectively, these findings highlight the therapeutic potential of IVA337 in reducing fibrosis and inflammation while simultaneously enhancing lipid metabolic reprogramming in activated HSCs from patients with MASH.

Transcriptomic Insights into the Response of MASH Patient HSCs to Pan-PPAR Agonist IVA337 Treatment

To elucidate the molecular mechanisms underlying the effects of IVA337 on activated HSCs from patients with MASH, comprehensive transcriptomic profiling was conducted. Initially, RNA sequencing was performed; significant alterations in gene expression were then analyzed and visualized through volcano plots for each donor. Differentially expressed genes (DEGs) are illustrated in the plots, and the top 10 up-regulated and down-regulated genes of each plot are annotated (Figure 2A). Notably, several genes associated with lipid metabolism, such as *PLIN2* and *ANGPTL4*, were prominently featured among the altered genes.

Functional analysis of DEGs (fold change >1.5) was conducted by using the KEGG database to identify affected pathways. Heatmaps illustrated DEG expression across donors, and the altered pathways were indicated accordingly (Figure 2B). As expected, the PPAR signaling pathway was significantly up-regulated after IVA337 treatment in both donors. Despite minor interindividual variability, consistent trends emerged; these included up-regulation of fatty acid metabolism pathways and down-

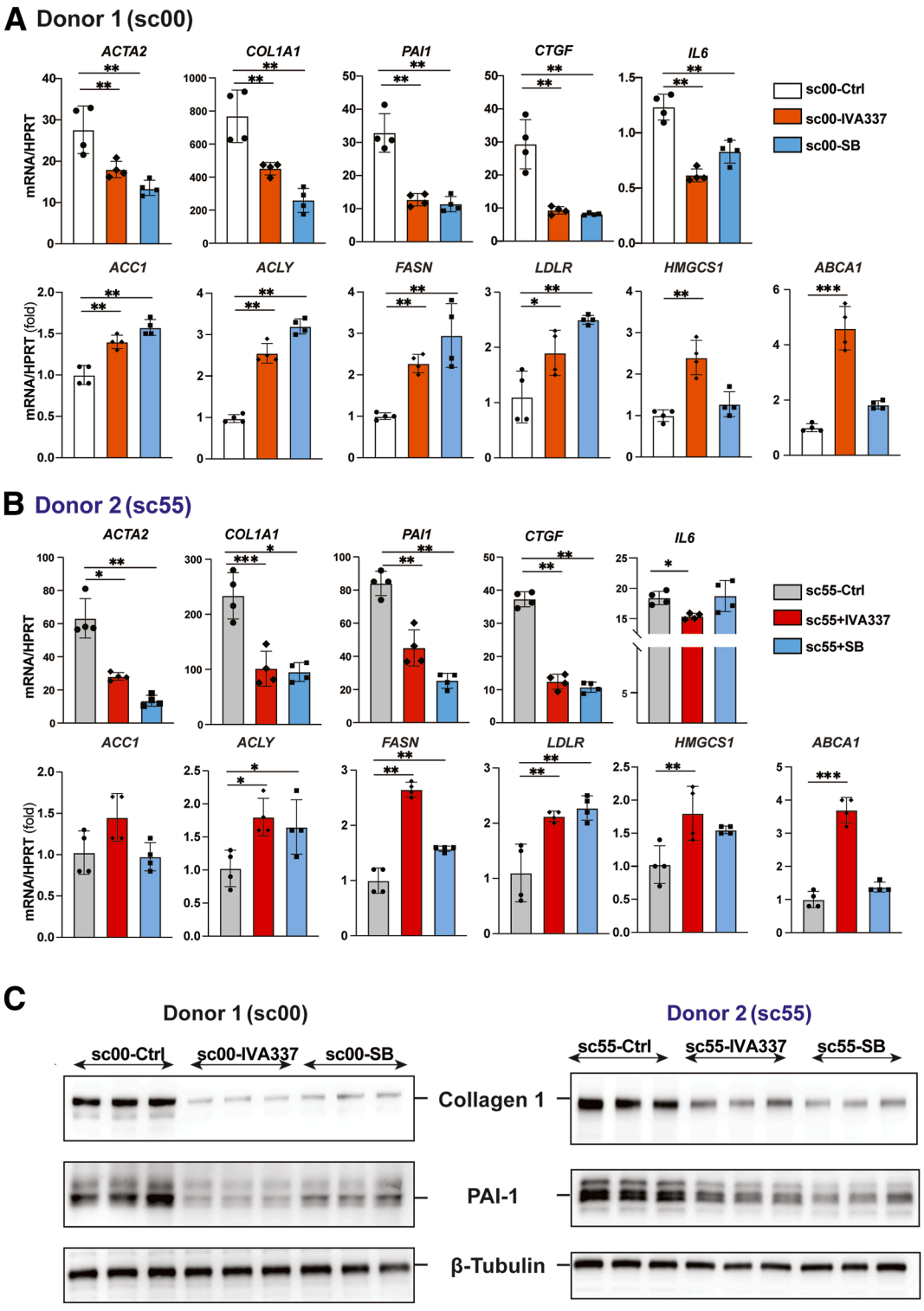

Figure 1 IVA337 (IVA) reduced the activated phenotype of hepatic stellate cells (HSCs) from human patients with metabolic dysfunction—associated steatohepatitis (MASH). **A:** HSCs isolated from MASH patient donor 1 (sc00) were treated with IVA or SB431542 (SB). mRNA expression of fibrosis-, inflammation-, and lipid metabolism—related genes was assessed by quantitative real-time PCR. **B:** Similar quantitative real-time PCR analysis was performed with HSCs from another MASH patient (donor 2, sc55). *HPRT* mRNA was used as internal control. **C:** Protein expression of fibrogenic markers in patient HSCs was evaluated by Western blot analysis, and beta-tubulin was used as a loading control. Data are expressed as means ± SEM. $*P < 0.05$; $**P < 0.01$; $***P < 0.001$ (one-way analysis of variance).

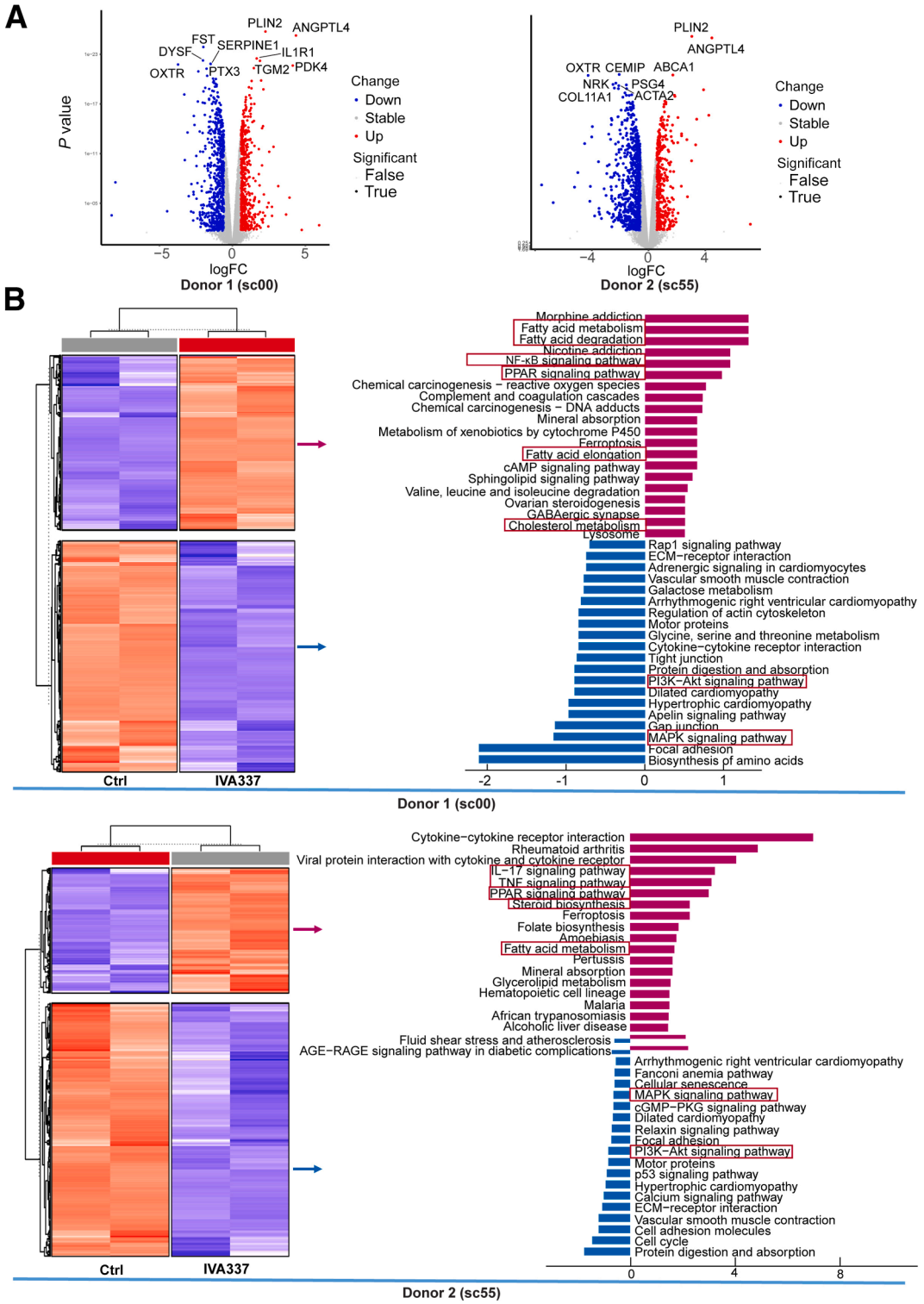

Figure 2 RNA-sequencing results with Gene Ontology (GO) functional analysis of hepatic stellate cells (HSCs) from two different metabolic dysfunction–associated steatohepatitis (MASH) patient donors after IVA337 treatment. **A:** Volcano plots present overviews of different expression genes between IVA337 versus control (ctrl) in individual HSCs from two donors, respectively. The threshold was fold change (FC) >1.5 and $P < 0.05$. **Red dots** indicate up-regulated genes in IVA337 treatment; **blue dots** indicate down-regulated genes; and **gray dots** indicate nonsignificant genes in IVA337 treatment. **B:** Heatmap of up-regulated and down-regulated differentially expressed genes of different donors and GO analysis upon IVA337 treatment, respectively. Block diagrams showing the most differentially expressed functional pathways based on the GO database. The **red block** indicates up-regulated differentially expressed genes in the IVA337 group, and the **blue block** indicates down-regulated ones. The length of the block represents the number of genes that mapped to this GO term. AGE-RAGE, advanced glycation end product–receptor for advanced glycation end product; cGMP-PKG, cGMP–protein kinase G; ECM, extracellular matrix; MAPK, mitogen-activated protein kinase; PI3K-AKT, phosphatidylinositol 3kinase–protein kinase B; PPAR, peroxisome proliferator–activated receptor.

regulation in mitogen-activated protein kinase (MAPK) and phosphatidylinositol 3kinase (PI3K)/protein kinase B (AKT) signaling pathways, which were prominent. These findings were further validated by Gene Set Enrichment Analysis, which confirmed significant pathway enrichments (Supplemental Figures S1 and S2).

In conjunction with KEGG analysis, this work focused on validating critical genes involved in pathways implicated in MASH progression, including inflammation and cholesterol and lipid metabolism, as well as key signaling pathways such as MAPK, PI3K-AKT, Janus kinase−STAT, and AMP-activated protein kinase. The potential DEGs are presented in a heatmap (Figure 3A). The heatmap shows that treatment with IVA337 resulted in the up-regulation of genes related to cholesterol and lipid metabolism, while down-regulating genes associated with MAPK, PI3K-AKT, and Janus kinase−STAT signaling pathways.

To validate RNA-sequencing findings, eight DEGs from the lipid metabolism and MAPK and PI3K-AKT signaling pathways were selected to verify their expression by quantitative RT-PCR. Validation confirmed the RNA-sequencing results, showing a significant modulation of gene expression posttreatment: increases of approximately twofold were observed in *ACAA2, FADS1*, and *CPT1A*, all key players in lipid metabolism; a decrease of about 1.5-fold was noted in *ACOT7*. In contrast, genes associated with the MAPK signaling pathway (*MAP3K7CL* and *PDGFA*) and the PI3K-AKT pathway (*NR4A1* and *RASSF7*) showed decreases, with fold changes ranging from 2 to 3 (Figure 3B).

The top DEGs associated with lipid metabolism were further validated. As shown in Figure 4A, the mRNA levels of *ANGPTL4* and *PLIN2* in human HSCs were significantly increased after treatment with IVA337 but not with SB431542. Because ANGPTL4 functions as a serum hormone−regulating lipid metabolism, we focused on the protein expression of PLIN2. Western blot analysis revealed that PLIN2 protein levels were markedly elevated in both MASH donor HSCs after IVA337 treatment. Given that PLIN2 is a key lipid droplet−associated protein involved in cholesterol-containing lipid droplets, immunofluorescence staining was used to visualize its location and expression *in vivo*. As shown in Figure 4B, treatment with IVA337 increased the spread of PLIN2 in MASH HSCs, and the lipid droplets appeared more prominent.

The transcriptomic profiling, supported by validation, provides valuable insights into the molecular mechanisms by which IVA337 modulates the pathologic activation of HSCs in patients with MASH.

IVA337 Ameliorates Fibrosis and Inflammation of in Mouse Liver Spheroids by Modulating Lipid Metabolism

To determine whether the pathways altered in HSCs during MASH progression are similarly affected in a murine model, 3D liver spheroids were used, offering a more physiologically relevant model than traditional two-dimensional cultures. Morphology and prefibrotic state of these spheroids were assessed via immunofluorescence. Under MASH-inducing conditions, the mouse spheroids exhibited enhanced co-expression of collagen 1 (COL1) and hepatocyte nuclear factor 4α (HNF4A). Treatment with IVA337 and SB431542 markedly reduced the expression of COL1 and its co-localization with HNF4A (Figure 5A). In addition, lipid accumulation within the spheroids, visualized via BODIPY staining, was significantly higher in the IVA337-treated groups compared with the MASH-only spheroids (Figure 5A).

Further molecular analysis was conducted to probe the underlying mechanisms. qPCR revealed elevated expression of the fibrosis marker *ACAT2* in the MASH spheroids relative to controls, which was significantly attenuated by both IVA337 and SB431542. Similarly, the inflammation marker *IL6* was reduced after treatment with both reagents. In lipid metabolism, MASH spheroids exhibited down-regulation of key regulatory fatty acid metabolic enzymes, including *SCD*, *FADS1*, and *ACOT4*. IVA337 treatment restored these enzymes to near-normal levels, an effect not observed with SB431542 (Figure 4B). In addition, the expression of *ACAA2*, crucial for fatty acid oxidation, followed a similar pattern of down-regulation in MASH conditions and restoration with IVA337 treatment (Figure 5B). Moreover, the expression of *PCSK9*, an important regulator of cholesterol metabolism, was decreased under MASH conditions and was effectively reversed by IVA337 treatment. In contrast, the gene involved in the MAPK signaling pathway, *MAP3K7CL*, was up-regulated in MASH spheroids and was repressed by treatment with both IVA337 and SB431542 (Figure 5B).

These findings show that IVA337 not only inhibits fibrosis and inflammation in mouse liver spheroids but also restores dysregulated lipid metabolism and suppresses the activation of the MAPK signaling pathway.

Modulating Lipid Homeostasis by IVA337 in Human MASH Spheroids

To further evaluate the effects of IVA337 in a more disease-relevant model, 3D MASH spheroids were generated by using human hepatocytes, stellate cells, and NPCs derived from patients with MASH, then further cultured under normal and MASH-inducing conditions. As shown by immunofluorescence staining, collagen 1 and α-smooth muscle actin intensities were significantly reduced after IVA337 treatment, compared with the MASH induction condition. In contrast, BODIPY staining was increased with IVA337 treatment, surpassing levels observed in the MASH condition (Figure 6A).

The human spheroids were then subjected to RNA sequencing, which was performed in duplicate for each condition. The initial analysis focused on the MAPK

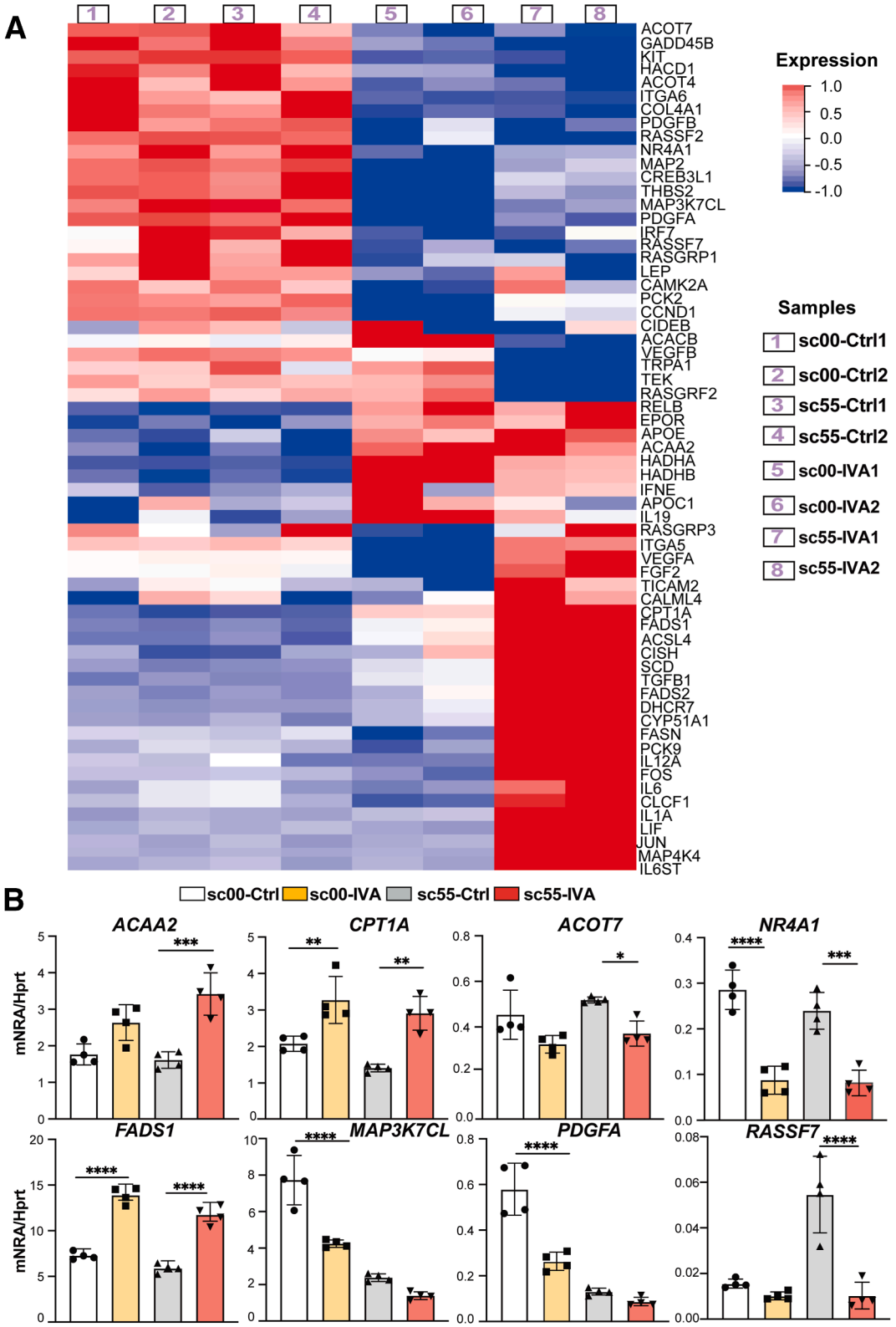

Figure 3 Potential deregulated gene identification after IVA337 (IVA) incubation. **A:** Heatmap of up-regulated and down-regulated genes (fold change at least in one group >1.5) between different treatments with hepatic primary stellate cells from two donors. **B:** Quantitative real-time PCR analysis of candidate deregulated genes' mRNA level with hepatic stellate cells from two donors. *HPRT* mRNA level was set as control (Ctrl). Relative mRNA levels are expressed as means ± SEM. *$P < 0.05$; **$P < 0.01$; ***$P < 0.001$; ****$P < 0.0001$ (one-way analysis of variance).

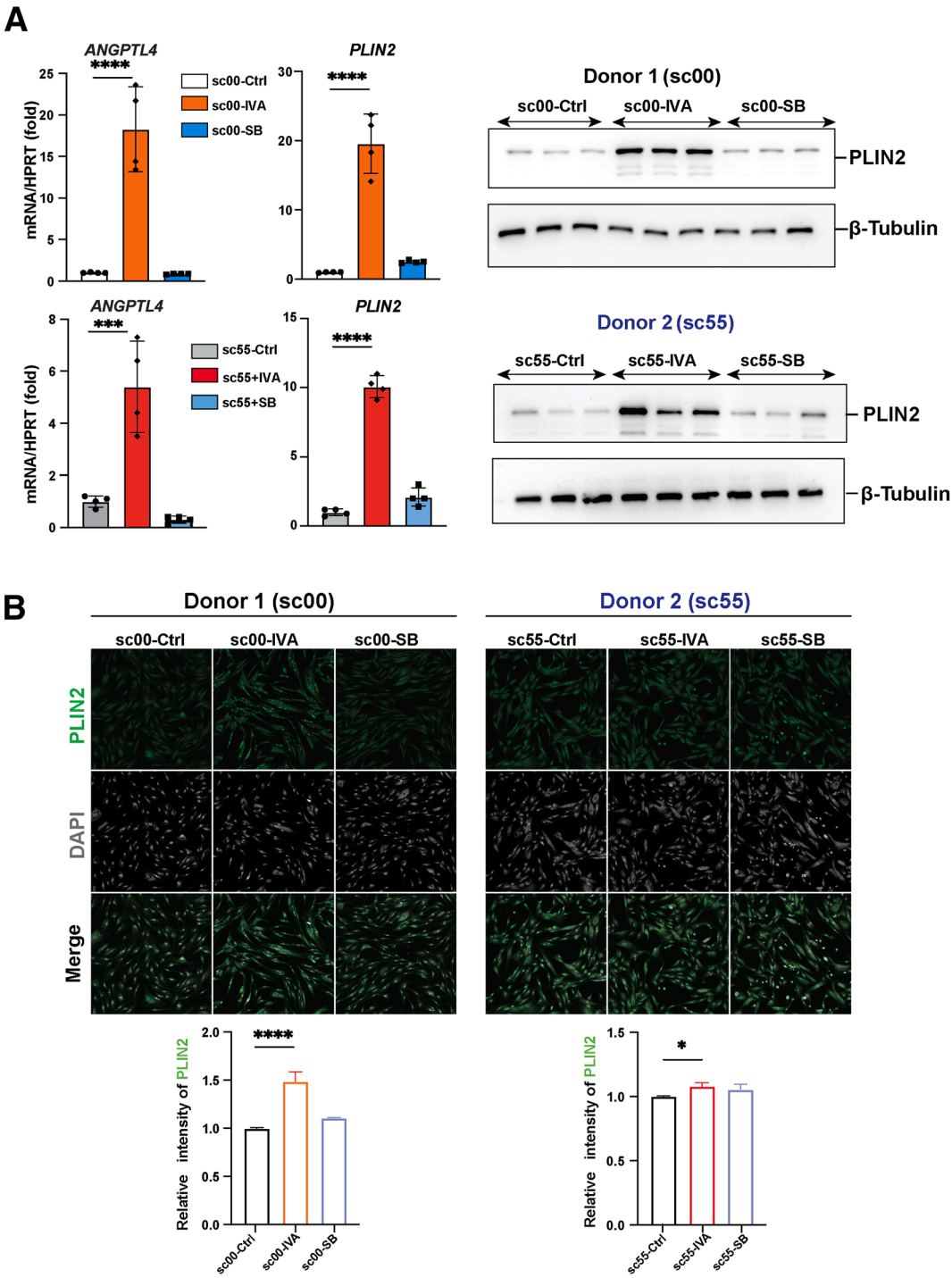

Figure 4 IVA337 (IVA) treatment significantly enhances the expression of lipid metabolism—related differentially expressed genes in hepatic stellate cells (HSCs) from patients with metabolic dysfunction—associated steatohepatitis. **A:** Relative mRNA levels of ANGPTL4 and PLIN2 in HSCs after treatment with IVA or SB431542 (SB). PLIN2 protein levels were assessed by Western blot analysis. *HPRT* mRNA was used as the internal control (Ctrl) for quantitative real-time PCR, and beta-tubulin served as the loading control for Western blot analysis. **B:** Immunofluorescence staining for PLIN2 (green) in HSCs derived from two patient donors with metabolic dysfunction—associated steatohepatitis after treatment with IVA or SB. Data are expressed as means ± SEM. $^{*}P < 0.05$; $^{***}P < 0.001$; $^{****}P < 0.0001$ (one-way analysis of variance). Original magnification: ×20; quantification of relative fluorescence intensity is shown in the **lower panel** (**B**).

pathway, previously identified as significantly altered after IVA337 treatment in both human HSCs and mouse spheroids. Positive regulation genes in the MAPK cascade were remarkably differently regulated in MASH versus controls, in which up-regulated and down-regulated genes were separately divided into two categories, whereas IVA377 could remarkably down-regulate some up-regulated genes in MASH spheroids. Transcriptional

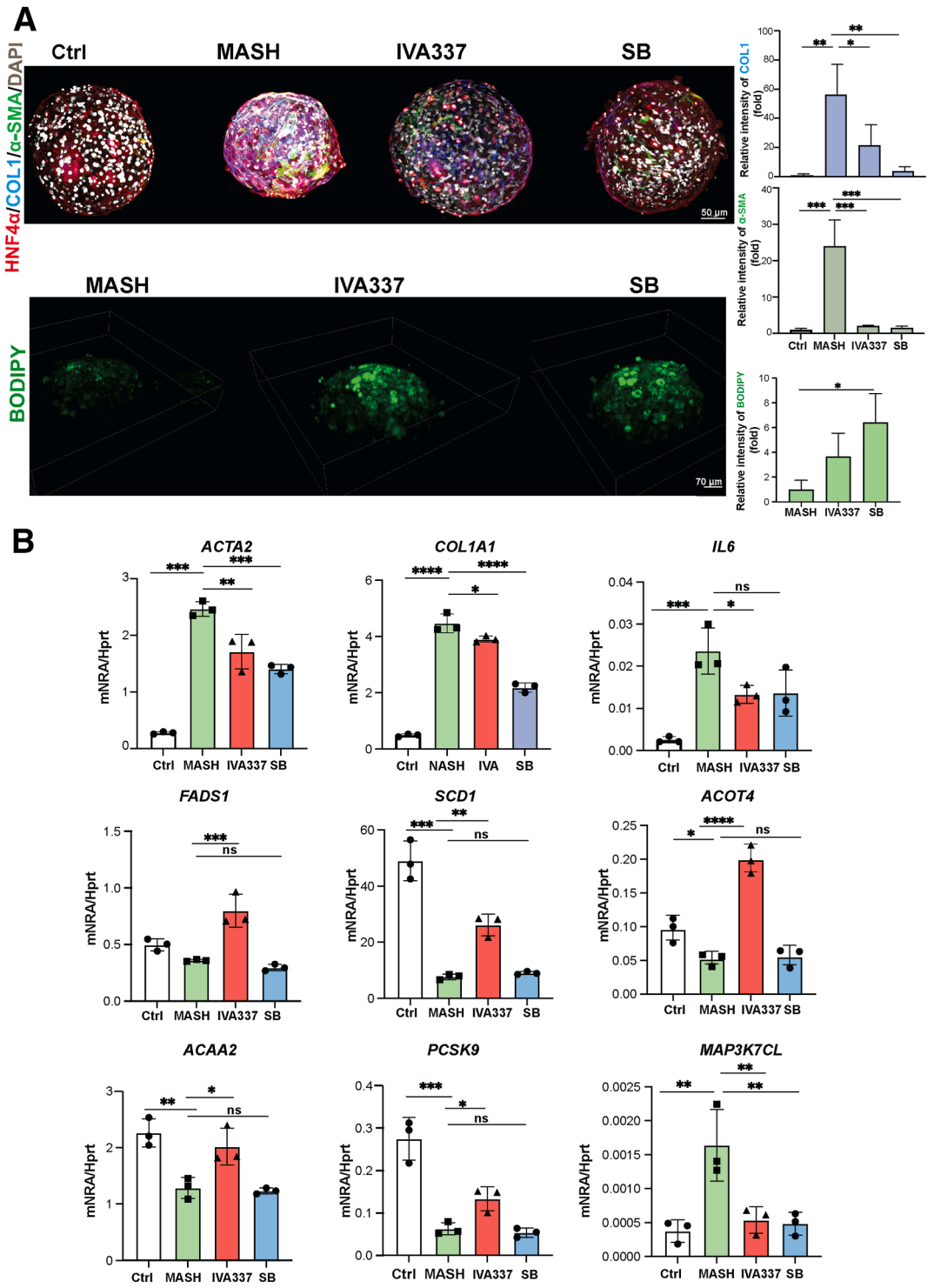

Figure 5 IVA337 inhibits metabolic dysfunction–associated steatohepatitis (MASH) progression in mouse spheroids by affecting lipid homeostasis and mitogen-activated protein kinase pathways. **A:** Generation of mouse spheroids and induction of MASH. Immunofluorescence showed that IVA337 effectively inhibited fibrosis as shown by decreasing collagen 1 (COL1) and α-smooth muscle actin (α-SMA) staining, and it promoted lipid storage as evidenced by BODIPY staining. The relative fluorescence intensities of COL1, α-SMA, and BODIPY are quantified in the **lower panel**. **B:** Quantitative real-time PCR analysis revealed that IVA337 treatment promoted the expression of genes related to lipid metabolism, including MUFA synthesis (*SCD* and *FADS1*), beta-oxidation (*ACAA2* and *ACOT4*), and cholesterol efflux (*PCSK9*). In addition, inflammation and fibrosis-related gene expression were significantly repressed. *HPRT* mRNA was used as the internal control. Data are expressed as means ± SEM. $^{*}P < 0.05$ $^{**}P < 0.01$; $^{***}P < 0.001$; $^{****}P < 0.0001$ (one-way analysis of variance test). Scale bar: 50 μm (α-SMA staining, **A**); 70 μm (BODIPY staining, **A**). ns, nonsignificant; SB, SB431542.

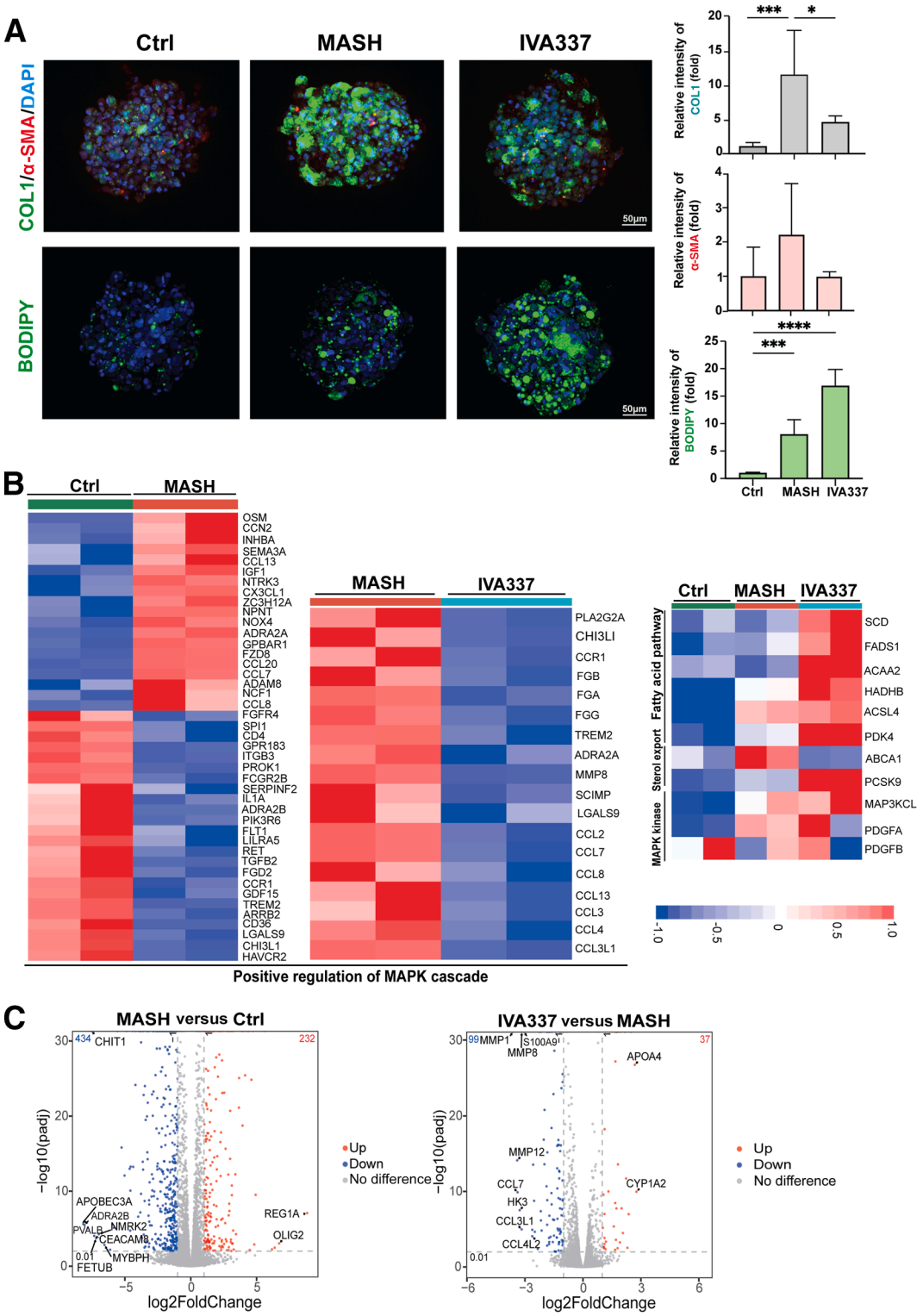

Figure 6 IVA337 ameliorated fibrosis in human metabolic dysfunction–associated steatohepatitis (MASH) spheroids by modulating lipid homeostasis. **A:** Generation of human spheroids and MASH induction. Representative immunofluorescence images of collagen 1 (COL1), α-smooth muscle actin (α-SMA), and BODIPY shows that IVA337 effectively inhibited fibrosis and enhanced lipid storage. Quantification of fluorescence intensities is shown in the **lower panel**. **B:** Heatmap analysis of gene expression profiles related to mitogen-activated protein kinase (MAPK) signaling, sterol export, and fatty acid pathway genes based on RNA-sequencing data from three-dimensional human spheroids. **C:** Volcano plots showing the difference in differentially expressed genes between MASH versus control (Ctrl) and IVA337 versus MASH groups. The threshold was fold change >2 and $P < 0.01$. **Red dots** indicate up-regulated genes, **blue dots** indicate down-regulated genes, and **gray dots** indicate nonsignificant changes. Data are expressed as means ± SEM. $^{*}P < 0.05$; $^{***}P < 0.001$; $^{****}P < 0.0001$ (one-way analysis of variance test). Scale bars = 50 μm (**A**).

profiling further revealed substantial modulation of pathways involved in fatty acid metabolism and sterol export. Heatmaps depicting the relative expression levels illustrated widespread deregulation of these genes in MASH spheroids, which were also substantially modulated after IVA337 treatment (Figure 6B).

A comprehensive bioinformatics analysis of global gene expression changes in human spheroids was also performed. It identified a total of 666 DEGs in the MASH group (232 up-regulated and 434 down-regulated) (fold change >2, $P < 0.01$), and 136 DEGs in the IVA337-treated group compared with MASH (37 up-regulated and 99 down-regulated), as shown in volcano plots (Figure 6C). The top 10 DEGs are highlighted in these plots.

Among the DEGs between the IVA337-treated and MASH groups, the up-regulated genes underwent Gene Ontology enrichment analysis and were categorized into groups of biological process, while the down-regulated genes were applied to KEGG enrichment analysis. The biological processes enriched mainly in fatty acid metabolic process, lipid catabolic, and metabolic process. The down-regulated genes mainly enriched in IL-17, lipid, NF-κB , and tumor necrosis factor signaling pathways (Supplemental Figure S3).

When comparing DEGs across MASH versus control and IVA337 versus MASH groups, 735 genes were identified as significantly altered (fold change >2, $P < 0.01$); 67 genes were common across all conditions. Subsequent pathway analysis of these 67 common DEGs using KEGG revealed significant pathways, including the PPAR signaling pathway, affirming the quality and relevance of the sequencing data (Figure 7A). Notably, pathways related to IL-17 signaling and lipid metabolism were also identified, indicating that IVA337 modulates these pathways to mitigate fibrosis and inflammation during MASH progression.

Moreover, the common 67 DEGs were clustered by using a hierarchical clustering algorithm and displayed in a heatmap (Figure 7B). Comparing the expression patterns of control, MASH, and IVA337 groups, some MASH-related genes categorized as different groups (group numbers 1 to 4) were restored to control-like expression levels after IVA337 treatment. KEGG pathway analysis on these restored genes underscored the lipid metabolism pathway as predominantly influenced by IVA337.

To further validate these findings, Western blot and qPCR analyses were performed by using newly generated human spheroids. As confirmed by Western blot analysis, the fibrosis markers collagen 1 and α-smooth muscle actin were markedly increased in MASH spheroids and significantly decreased after IVA337 treatment. In addition, PLIN2 levels were slightly elevated after IVA337 treatment compared with MASH, which was consistent with results from IVA337-treated HSC assays (Figure 7C).

The expression of fibrotic marker genes was also assessed by qPCR (Figure 7D). These results showed a significant reduction in *ACTA2*, *COL1A1* (approximately twofold), and *CTGF* (around threefold). Moreover, the mRNA levels of the inflammatory gene *IL6* were reduced by 50%, confirming that spheroid generation was successful and the phenotypic changes aligned with the sequencing data. Next, we assessed genes involved in fatty acid metabolism, finding that *FADS1* was significantly up-regulated after IVA337 treatment compared with MASH. In contrast, the MAPK pathway gene *MAP3K7CL* was repressed after IVA337 treatment.

The lipid droplet–associated protein *PLIN5* (Perilipin 5), which belongs to Group 4, was also examined and found that it was slightly restored upon IVA337 treatment (Figure 7D). Given that the IL-17 signaling pathway appeared to be modulated by IVA337 based on KEGG analysis, genes in this pathway were selected for further validation (Figure 7D). Notably, *CXCL8*, *CCL7*, and *MMP1*, which are also part of Group 3 expression patterns, were all significantly down-regulated by approximately twofold to threefold after IVA337 treatment, reaching levels similar to those of the controls.

These results highlight the crucial role of IVA337 in restoring lipid homeostasis and modulating inflammatory and metabolic pathways in human MASH spheroids.

Discussion

The pathogenesis of MASH is multifaceted, and, as a result, PPAR agonists have long been considered promising therapeutic candidates. IVA337 is currently the only PPAR agonist undergoing Phase III trials, showing beneficial effects in improving lipotoxicity and metabolic stress. In contrast, the PPARβ/δ agonist elafibranor failed in Phase III trials.[44] The current study directly applied IVA337 to HSCs derived from patients with MASH to evaluate its therapeutic effects while also investigating its role in mouse and human MASH 3D spheroids. The efficacy of IVA337 in both *in vitro* and *in vivo* models provides valuable insights into the potential pathways modulating lipid homeostasis through which PPAR agonists can mitigate the progression of MASH.

These study findings indicate that IVA337 significantly reduced the expression of fibrosis markers such as *ACTA2* and *COL1A1* in cultured human HSCs from MASH donors. This is consistent with earlier research showing the fibrosis-ameliorating effects of other PPAR agonists,[35] reinforcing their potential to significantly alter the fibrogenic landscape of the liver. In addition, IVA337 effectively suppressed inflammation, as evidenced by the dramatic inhibition of *IL-6* expression. These results extend previous studies, indicating that PPAR activation has a direct antifibrotic and anti-inflammatory effect in liver tissues.

One of the most notable findings of the current study is the ability of IVA337 to regulate lipid metabolism in HSCs,

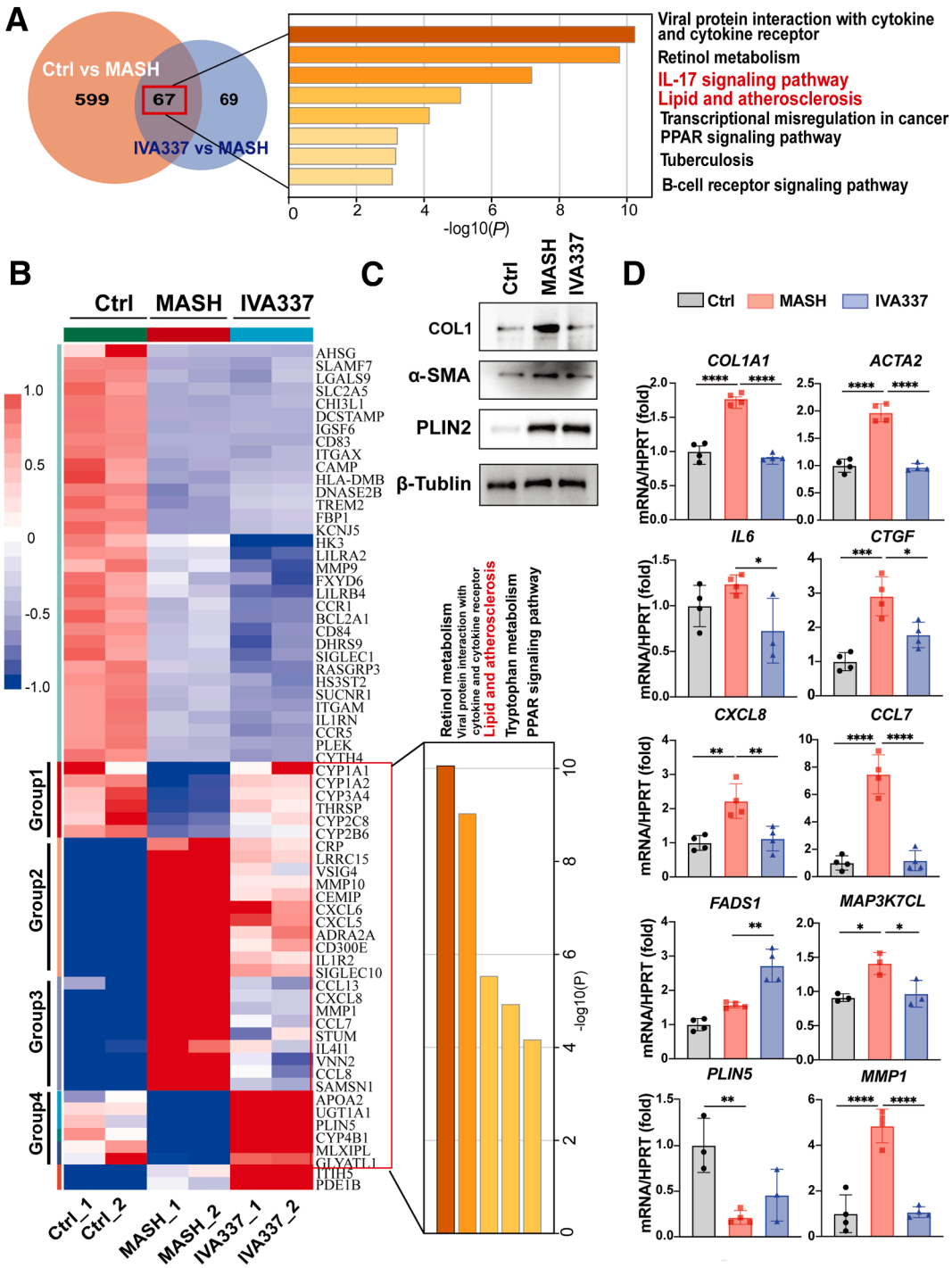

Figure 7 Kyoto Encyclopedia of Genes and Genomes (KEGG) pathway enrichment and validation of differentially expressed genes across treatment groups. **A:** Venn diagram and KEGG pathway analysis of commonly deregulated genes among control (Ctrl), metabolic dysfunction–associated steatohepatitis (MASH), and IVA337-treated groups. Pathways associated with IL-17 signaling and lipid metabolism process pathways were significantly enriched and are highlighted in red. **B:** Heatmap of 67 commonly regulated differentially expressed genes and corresponding KEGG pathway analysis in groups 1 to 4 (highlighted in **red box**). **C:** Protein expression of fibrosis markers and PLIN2 in human spheroids assessed by Western blot analysis. Beta-tubulin was a loading control. **D:** Validation of deregulated gene expression in human spheroids using quantitative real-time PCR. *HPRT* mRNA was used as the internal control. Data are expressed as means ± SEM, with $*P < 0.05$; $**P < 0.01$; $***P < 0.001$; $****P < 0.0001$ (one-way analysis of variance test). PPAR, peroxisome proliferator–activated receptor.

suggesting a novel approach to managing MASH. It is well established that harmful lipids produced by hepatocytes trigger several MASH-promoting signaling pathways, including HSC activation.[5] Clinical trials of lipid metabolism inhibitors have highlighted the critical role of hepatocyte lipid metabolism in initiating fibrosis-promoting hepatocyte-macrophage-HSC crosstalk in MASH.[45] Our data emphasized that the modulation of lipid homeostasis is

crucial, perhaps because lipid accumulation is a primary driver of HSC activation and subsequent fibrosis.

Key lipid metabolism genes whose expression was reversed by IVA337 treatment in MASH patient HSCs include *FADS1, ACAA2, CPT1A*, and *ACOT4/7*. FADS1 is the sole enzyme responsible for producing the important polyunsaturated fatty acids arachidonic acid and eicosapentaenoic acid, which are associated with obesity, dyslipidemia, and nonalcoholic fatty liver disease when muted or defected.[46] Knockdown of *FADS1* results in lipid accumulation in HepG2 cells, which can be reversed by overexpression of FADS1 or PPARα agonists in mice.[47] Acetyl-CoA acyltransferase 2 (ACAA2) is involved in mitochondrial fatty acid elongation and degradation by catalyzing the last step of the beta-oxidation pathway, with its down-regulation associated with hepatic steatosis and up-regulation showing protective effects.[48–51] CPT1A (carnitine palmitoyltransferase 1A), the key enzyme in fatty acid oxidation, can alter lipid profiles and reduce hepatic steatosis in MASLD mouse models.[52] ACOT7, a member of the Acyl-CoA thioesterase (ACOT) family, regulates fatty acid metabolism and promotes hepatocellular carcinoma,[53] similarly to ACOT4, which modulates lipid metabolism via AMP-activated protein kinase and AKT activity in hepatocytes.[54] By reversing the activity of these enzymes, IVA337 helps restore normal lipid metabolism, thereby preventing HSC activation and potentially reversing fibrogenic pathways. Furthermore, IVA337 treatment led to increased lipid accumulation, as evidenced by BODIPY staining and elevated levels of lipid droplets, indicated by up-regulation of PLIN2. This increase may reflect an adaptive response to imbalanced fatty acid supply and turnover, as lipid accumulation and lipid droplet biogenesis are generally considered protective mechanisms in the early stages of cellular stress.[55]

Transcription profiling of HSCs and 3D human spheroids provided deeper insights into the molecular effects of IVA337. Genes involved in fatty acid metabolism were consistently up-regulated in both HSCs and human spheroids after IVA337 treatment, while cholesterol metabolism was up-regulated in MASH HSCs post-IVA337 incubation. Notably, many genes up-regulated by IVA337 in HSCs were enriched in IL-17, NF-κB, and tumor necrosis factor signaling pathways. In human spheroids, several common genes mediated by IVA337 were significantly attributed to IL-17 signaling. Furthermore, many genes down-regulated by IVA337 in human spheroids were enriched in NF-κB and tumor necrosis factor signaling pathways. Some distinct signaling pathways were enriched between HSCs and spheroids, such as PI3K-AKT and MAPK pathways, which showed significant changes in HSCs but not in spheroids.

Overall, the up-regulation of genes involved in beta-oxidation and the corresponding up-regulation of genes associated with lipid export promote a shift toward a healthier metabolic status post-IVA337 treatment. Several signaling pathways, including IL-17, tumor necrosis factor, NF-κB, PI3K-AKT, and MAPK, may play crucial roles in this process. These findings are particularly relevant, given the central role of dysregulated lipid metabolism in MASH pathogenesis, and they underscore the potential of PPAR agonists to restore metabolic balance. Future studies should explore combination therapies to enhance therapeutic outcomes in patients with MASH. Perhaps combining IVA337 with agents targeting lipid metabolism or IL-17 or other signaling pathways identified in this study may offer a more comprehensive strategy for treating liver diseases, potentially leading to improved clinical outcomes.

Acknowledgments

We thank Prof. Dr. Jinsong Li (CAS Center for Excellence in Molecular Cell Science, Shanghai Institute of Biochemistry and Cell Biology) for valuable suggestions on the manuscript; Karin Diggle from Dr. Kisseleva's group at the University of California San Diego for her excellent organization support during performance of experiments; and YZcell Biotechnology Inc. Company (Xiamen, China) for technical assistance of primary mouse liver cell isolation or construction of the liver spheroids. The graphic abstract was created with BioRender.com (Toronto, ON, Canada).

Author Contributions

N.L. and X. Liu conceptualized the study; M.Y. analyzed the data; N.L. acquired funding; N.L., S.W., X. Li, Y.D., and X. Liu performed experiments; S.W. and X. Liu developed methods; M.Y. provided software; N.L. and T.K. supervised the study; N.L. wrote the manuscript; and L.Z., D.A.B., T.K., and X. Liu reviewed and edited the manuscript.

Disclosure Statement

None declared.

Supplemental Data

Supplemental material for this article can be found at *https://doi.org/10.1016/j.ajpath.2025.06.012*.

References

1. Le MH, Yeo YH, Li X, Li J, Zou B, Wu Y, Ye Q, Huang DQ, Zhao C, Zhang J, Liu C, Chang N, Xing F, Yan S, Wan ZH, Tang NSY, Mayumi M, Liu X, Liu C, Rui F, Yang H, Yang Y, Jin R, Le RHX, Xu Y, Le DM, Barnett S, Stave CD, Cheung R, Zhu Q, Nguyen MH: 2019 Global NAFLD prevalence: a systematic review and meta-analysis. Clin Gastroenterol Hepatol 2022, 20:2809–2817.e28
2. Musso G, Cassader M, Gambino R: Non-alcoholic steatohepatitis: emerging molecular targets and therapeutic strategies. Nat Rev Drug Discov 2016, 15:249–274

3. Muzio G, Barrera G, Pizzimenti S: Peroxisome proliferator-activated receptors (PPARs) and oxidative stress in physiological conditions and in cancer. Antioxidants (Basel) 2021, 10:1734
4. Loomba R, Friedman SL, Shulman GI: Mechanisms and disease consequences of nonalcoholic fatty liver disease. Cell 2021, 184: 2537−2564
5. Schwabe RF, Tabas I, Pajvani UB: Mechanisms of fibrosis development in nonalcoholic steatohepatitis. Gastroenterology 2020, 158: 1913−1928
6. Tsuchida T, Friedman SL: Mechanisms of hepatic stellate cell activation. Nat Rev Gastroenterol Hepatol 2017, 14:397−411
7. Singh S, Allen AM, Wang Z, Prokop LJ, Murad MH, Loomba R: Fibrosis progression in nonalcoholic fatty liver vs nonalcoholic steatohepatitis: a systematic review and meta-analysis of paired-biopsy studies. Clin Gastroenterol Hepatol 2015, 13:643−654.e1-9. quiz e39-40
8. Harrison SA, Bedossa P, Guy CD, Schattenberg JM, Loomba R, Taub R, Labriola D, Moussa SE, Neff GW, Rinella ME, Anstee QM, Abdelmalek MF, Younossi Z, Baum SJ, Francque S, Charlton MR, Newsome PN, Lanthier N, Schiefke I, Mangia A, Pericàs JM, Patil R, Sanyal AJ, Noureddin M, Bansal MB, Alkhouri N, Castera L, Rudraraju M, Ratziu V; MAESTRO-NASH Investigators: A phase 3, randomized, controlled trial of resmetirom in NASH with liver fibrosis. N Engl J Med 2024, 390:497−509
9. Changizi Z, Kajbaf F, Moslehi A: An overview of the role of peroxisome proliferator-activated receptors in liver diseases. J Clin Transl Hepatol 2023, 11:1542−1552
10. Inagaki T, Dutchak P, Zhao G, Ding X, Gautron L, Parameswara V, Li Y, Goetz R, Mohammadi M, Esser V, Elmquist JK, Gerard RD, Burgess SC, Hammer RE, Mangelsdorf DJ, Kliewer SA: Endocrine regulation of the fasting response by PPARalpha-mediated induction of fibroblast growth factor 21. Cell Metab 2007, 5:415−425
11. Kersten S, Mandard S, Tan NS, Escher P, Metzger D, Chambon P, Gonzalez FJ, Desvergne B, Wahli W: Characterization of the fasting-induced adipose factor FIAF, a novel peroxisome proliferator-activated receptor target gene. J Biol Chem 2000, 275:28488−28493
12. Kersten S, Seydoux J, Peters JM, Gonzalez FJ, Desvergne B, Wahli W: Peroxisome proliferator-activated receptor alpha mediates the adaptive response to fasting. J Clin Invest 1999, 103:1489−1498
13. Gross B, Pawlak M, Lefebvre P, Staels B: PPARs in obesity-induced T2DM, dyslipidaemia and NAFLD. Nat Rev Endocrinol 2017, 13: 36−49
14. Wang Y-X, Zhang C-L, Yu RT, Cho HK, Nelson MC, Bayuga-Ocampo CR, Ham J, Kang H, Evans RM: Regulation of muscle fiber type and running endurance by PPARdelta. PLoS Biol 2004, 2:e294
15. Liu S, Hatano B, Zhao M, Yen C-C, Kang K, Reilly SM, Gangl MR, Gorgun C, Balschi JA, Ntambi JM, Lee C-H: Role of peroxisome proliferator-activated receptor [delta]/[beta] in hepatic metabolic regulation. J Biol Chem 2011, 286:1237−1247
16. Iwaisako K, Haimerl M, Paik Y-H, Taura K, Kodama Y, Sirlin C, Yu E, Yu RT, Downes M, Evans RM, Brenner DA, Schnabl B: Protection from liver fibrosis by a peroxisome proliferator-activated receptor [delta] agonist. Proc Natl Acad Sci U S A 2012, 109: E1369−E1376
17. Zisser A, Ipsen DH, Tveden-Nyborg P: Hepatic stellate cell activation and inactivation in NASH-fibrosis-roles as putative treatment targets? Biomedicines 2021, 9:365
18. Hu W, Jiang C, Kim M, Xiao Y, Richter HJ, Guan D, Zhu K, Krusen BM, Roberts AN, Miller J, Steger DJ, Lazar MA: Isoform-specific functions of PPAR[gamma] in gene regulation and metabolism. Genes Dev 2022, 36:300−312
19. Knight BL, Hebbachi A, Hauton D, Brown A-M, Wiggins D, Patel DD, Gibbons GF: A role for PPARalpha in the control of SREBP activity and lipid synthesis in the liver. Biochem J 2005, 389:413−421
20. Ruiz R, Jideonwo V, Ahn M, Surendran S, Tagliabracci VS, Hou Y, Gamble A, Kerner J, Irimia-Dominguez JM, Puchowicz MA, DePaoli-Roach A, Hoppel C, Roach P, Morral N: Sterol regulatory element-binding protein-1 (SREBP-1) is required to regulate glycogen synthesis and gluconeogenic gene expression in mouse liver. J Biol Chem 2014, 289:5510−5517
21. Ide T, Shimano H, Yoshikawa T, Yahagi N, Amemiya-Kudo M, Matsuzaka T, Nakakuki M, Yatoh S, Iizuka Y, Tomita S, Ohashi K, Takahashi A, Sone H, Gotoda T, Osuga J, Ishibashi S, Yamada N: Cross-talk between peroxisome proliferator-activated receptor (PPAR) alpha and liver X receptor (LXR) in nutritional regulation of fatty acid metabolism. II. LXRs suppress lipid degradation gene promoters through inhibition of PPAR signaling. Mol Endocrinol 2003, 17:1255−1267
22. Monroy-Ramirez HC, Galicia-Moreno M, Sandoval-Rodriguez A, Meza-Rios A, Santos A, Armendariz-Borunda J: PPARs as metabolic sensors and therapeutic targets in liver diseases. Int J Mol Sci 2021, 22:8298
23. Kim JB, Wright HM, Wright M, Spiegelman BM: ADD1/SREBP1 activates PPARgamma through the production of endogenous ligand. Proc Natl Acad Sci U S A 1998, 95:4333−4337
24. Komeili-Movahhed T, Bassirian M, Changizi Z, Moslehi A: SIRT1/NF[kappa]B pathway mediates anti-inflammatory and anti-apoptotic effects of rosmarinic acid on in a mouse model of nonalcoholic steatohepatitis (NASH). J Recept Signal Transduct Res 2022, 42:241−250
25. El-Haggar SM, Mostafa TM: Comparative clinical study between the effect of fenofibrate alone and its combination with pentoxifylline on biochemical parameters and liver stiffness in patients with non-alcoholic fatty liver disease. Hepatol Int 2015, 9:471−479
26. Boeckmans J, Natale A, Rombaut M, Buyl K, Rogiers V, De Kock J, Vanhaecke T, Rodrigues RM: Anti-NASH drug development hitches a lift on PPAR agonism. Cells 2019, 9:37
27. Lee MY, Choi R, Kim HM, Cho EJ, Kim BH, Choi YS, Naowaboot J, Lee EY, Yang YC, Shin JY, Shin YG, Chung CH: Peroxisome proliferator-activated receptor [delta] agonist attenuates hepatic steatosis by anti-inflammatory mechanism. Exp Mol Med 2012, 44:578−585
28. Bajaj M, Suraamornkul S, Piper P, Hardies LJ, Glass L, Cersosimo E, Pratipanawatr T, Miyazaki Y, DeFronzo RA: Decreased plasma adiponectin concentrations are closely related to hepatic fat content and hepatic insulin resistance in pioglitazone-treated type 2 diabetic patients. J Clin Endocrinol Metab 2004, 89:200−206
29. Xi Y, Zhang Y, Zhu S, Luo Y, Xu P, Huang Z: PPAR-mediated toxicology and applied pharmacology. Cells 2020, 9:352
30. Lloyd S, Hayden MJ, Sakai Y, Fackett A, Silber PM, Hewitt NJ, Li AP: Differential in vitro hepatotoxicity of troglitazone and rosiglitazone among cryopreserved human hepatocytes from 37 donors. Chem Biol Interact 2002, 142:57−71
31. Ge J, Miao J-J, Sun X-Y, Yu J-Y: Huangkui capsule, an extract from Abelmoschus manihot (L.) medic, improves diabetic nephropathy via activating peroxisome proliferator-activated receptor (PPAR)-[alpha]/[gamma] and attenuating endoplasmic reticulum stress in rats. J Ethnopharmacol 2016, 189:238−249
32. Park MH, Kim DH, Kim MJ, Lee EK, An HJ, Jeong JW, Kim HR, Kim SJ, Yu BP, Moon HR, Chung HY: Effects of MHY908, a new synthetic PPAR[alpha]/[gamma] dual agonist, on inflammatory responses and insulin resistance in aged rats. J Gerontol A Biol Sci Med Sci 2016, 71:300−309
33. Ratziu V, Harrison SA, Francque S, Bedossa P, Lehert P, Serfaty L, Romero-Gomez M, Boursier J, Abdelmalek M, Caldwell S, Drenth J, Anstee QM, Hum D, Hanf R, Roudot A, Megnien S, Staels B, Sanyal A; GOLDEN-505 Investigator Study Group: Elafibranor, an agonist of the peroxisome proliferator-activated receptor-[alpha] and -[delta], induces resolution of nonalcoholic steatohepatitis without fibrosis worsening. Gastroenterology 2016, 150:1147−1159.e5
34. Kamata S, Honda A, Ishikawa R, Akahane M, Fujita A, Kaneko C, Miyawaki S, Habu Y, Shiiyama Y, Uchii K, Machida Y, Oyama T,

Ishii I: Functional and structural insights into the human PPAR [alpha]/[delta]/[gamma] targeting preferences of anti-NASH investigational drugs, lanifibranor, seladelpar, and elafibranor. Antioxidants (Basel) 2023, 12:1523
35. Wettstein G, Luccarini JM, Poekes L, Faye P, Kupkowski F, Adarbes V, Defrêne E, Estivalet C, Gawronski X, Jantzen I, Philippot A, Tessier J, Tuyaa-Boustugue P, Oakley F, Mann DA, Leclercq I, Francque S, Konstantinova I, Broqua P, Junien J-L: The new-generation pan-peroxisome proliferator-activated receptor agonist IVA337 protects the liver from metabolic disorders and fibrosis. Hepatol Commun 2017, 1:524−537
36. Lefere S, Puengel T, Hundertmark J, Penners C, Frank AK, Guillot A, de Muynck K, Heymann F, Adarbes V, Defrêne E, Estivalet C, Geerts A, Devisscher L, Wettstein G, Tacke F: Differential effects of selective- and pan-PPAR agonists on experimental steatohepatitis and hepatic macrophages. J Hepatol 2020, 73:757−770
37. Francque SM, Bedossa P, Ratziu V, Anstee QM, Bugianesi E, Sanyal AJ, Loomba R, Harrison SA, Balabanska R, Mateva L, Lanthier N, Alkhouri N, Moreno C, Schattenberg JM, Stefanova-Petrova D, Vonghia L, Rouzier R, Guillaume M, Hodge A, Romero-Gómez M, Huot-Marchand P, Baudin M, Richard M-P, Abitbol J-L, Broqua P, Junien J-L, Abdelmalek MF; NATIVE Study Group: A randomized, controlled trial of the pan-PPAR agonist lanifibranor in NASH. N Engl J Med 2021, 385:1547−1558
38. Kim HY, Lee W, Liu X, Jang H, Sakane S, Carvalho-Gontijo Weber R, Diggle K, Kerk SA, Metallo CM, Kisseleva T, Brenner DA: Protocol to generate human liver spheroids to study liver fibrosis induced by metabolic stress. STAR Protoc 2024, 5:103111
39. Liu X, Lam K, Zhao H, Sakane S, Kim HY, Eguileor A, Diggle K, Wu S, Gontijo Weber RC, Soroosh P, Hosseini M, Mekeel K, Brenner DA, Kisseleva T: Isolation of primary human liver cells from normal and nonalcoholic steatohepatitis livers. STAR Protoc 2023, 4:102391
40. Liu X, Xu J, Rosenthal S, Zhang L-J, McCubbin R, Meshgin N, Shang L, Koyama Y, Ma H-Y, Sharma S, Heinz S, Glass CK, Benner C, Brenner DA, Kisseleva T: Identification of lineage-specific transcription factors that prevent activation of hepatic stellate cells and promote fibrosis resolution. Gastroenterology 2020, 158:1728−1744.e14
41. Renier N, Wu Z, Simon DJ, Yang J, Ariel P, Tessier-Lavigne M: iDISCO: a simple, rapid method to immunolabel large tissue samples for volume imaging. Cell 2014, 159:896−910
42. Wiering L, Subramanian P, Hammerich L: Hepatic stellate cells: dictating outcome in nonalcoholic fatty liver disease. Cell Mol Gastroenterol Hepatol 2023, 15:1277−1292
43. Zhang J, Li R, Liu Q, Zhou J, Huang H, Huang Y, Zhang Z, Wu T, Tang Q, Huang C, Zhao Y, Zhang G, Mo L, Li Y, He J: SB431542-loaded liposomes alleviate liver fibrosis by suppressing TGF-[beta] signaling. Mol Pharm 2020, 17:4152−4162
44. Yang Y-Y, Xie L, Zhang N-P, Zhou D, Liu T-T, Wu J: Updates on novel pharmacotherapeutics for the treatment of nonalcoholic steatohepatitis. Acta Pharmacol Sin 2022, 43:1180−1190
45. Friedman SL, Neuschwander-Tetri BA, Rinella M, Sanyal AJ: Mechanisms of NAFLD development and therapeutic strategies. Nat Med 2018, 24:908−922
46. Gromovsky AD, Schugar RC, Brown AL, Helsley RN, Burrows AC, Ferguson D, Zhang R, Sansbury BE, Lee RG, Morton RE, Allende DS, Parks JS, Spite M, Brown JM: [delta]-5 fatty acid desaturase FADS1 impacts metabolic disease by balancing proinflammatory and proresolving lipid mediators. Arterioscler Thromb Vasc Biol 2018, 38:218−231
47. Athinarayanan S, Fan Y-Y, Wang X, Callaway E, Cai D, Chalasani N, Chapkin RS, Liu W: Fatty acid desaturase 1 influences hepatic lipid homeostasis by modulating the PPAR[alpha]-FGF21 axis. Hepatol Commun 2020, 5:461−477
48. He W, Li Q, Li X: Acetyl-CoA regulates lipid metabolism and histone acetylation modification in cancer. Biochim Biophys Acta Rev Cancer 2023, 1878:188837
49. Wu D, Liao G, Yao Y, Huang L, Dong B, Ma Y, Yang G: Down-regulated acetyl-CoA acyltransferase 2 promoted the progression of hepatocellular carcinoma and participated in the formation of immunosuppressive microenvironment. J Hepatocell Carcinoma 2023, 10:1327−1339
50. Agarwal N, Iyer D, Gabbi C, Saha P, Patel SG, Mo Q, Chang B, Goswami B, Schubert U, Kopp JB, Lewis DE, Balasubramanyam A: HIV-1 viral protein R (Vpr) induces fatty liver in mice via LXR [alpha] and PPAR[alpha] dysregulation: implications for HIV-specific pathogenesis of NAFLD. Sci Rep 2017, 7:13362
51. Lei X, Xu Q, Li C, Niu B, Ming Y, Li J, Tang Y, Li X, Tang J, Wu J, Ju Y, Yao L, Wang B, Miao Q, Zhong W, Zhi Y, Xu L, Li C, Li X, Mao Y: Egr1 confers protection against acetaminophen-induced hepatotoxicity via transcriptional upregulating of Acaa2. Int J Biol Sci 2022, 18:3800−3817
52. Weber M, Mera P, Casas J, Salvador J, Rodríguez A, Alonso S, Sebastián D, Soler-Vázquez MC, Montironi C, Recalde S, Fucho R, Calderón-Domínguez M, Mir JF, Bartrons R, Escola-Gil JC, Sánchez-Infantes D, Zorzano A, Llorente-Cortes V, Casals N, Valenti V, Frühbeck G, Herrero L, Serra D: Liver CPT1A gene therapy reduces diet-induced hepatic steatosis in mice and highlights potential lipid biomarkers for human NAFLD. FASEB J 2020, 34:11816−11837
53. Xie X, Chen C, Feng S, Zuo S, Zhao X, Li H: Acyl-CoA thioesterase 7 is transcriptionally activated by Krüppel-like factor 13 and promotes the progression of hepatocellular carcinoma. J Hepatocell Carcinoma 2021, 8:1623−1641
54. Yuan Q, Zhang X, Yang X, Zhang Q, Wei X, Ding Z, Chen J, Hua H, Huang D, Xu Y, Wang X, Gao C, Liu S, Zhang H: Knockdown of ACOT4 alleviates gluconeogenesis and lipid accumulation in hepatocytes. Heliyon 2024, 10:e27618
55. Zadoorian A, Du X, Yang H: Lipid droplet biogenesis and functions in health and disease. Nat Rev Endocrinol 2023, 19:443−459